Supplementary Information

Dynamic Nuclear Polarization Efficiency Increased by Very Fast Magic Angle Spinning

Sachin R. Chaudhari,[1]†‡ Dorothea Wisser,[1]‡ Arthur C. Pinon,[2] Pierrick Berruyer,[1] David Gajan,[1] Paul Tordo,[3] Olivier Ouari,[3] Christian Reiter,[4] Frank Engelke,[4] Christophe Copéret,[5] Moreno Lelli,[6*] Anne Lesage,[1*] and Lyndon Emsley[2*]

[1]Institut de Sciences Analytiques, Centre de RMN à Très Hauts Champs, Université de Lyon (CNRS/ENS Lyon/UCB Lyon 1), 69100 Villeurbanne, France; [2]Institut des Sciences et Ingénierie Chimiques, Ecole Polytechnique Fédérale de Lausanne (EPFL), CH-1015 Lausanne, Switzerland; [3]Aix-Marseille Univ, CNRS, ICR UMR 7273, 13397 Marseille, France; [4]Bruker Biospin, 76287 Rheinstetten, Germany, [5]ETH Zürich, Department of Chemistry and Applied Biosciences, Vladimir Prelog Weg 1-5, CH–8093 Zürich, Switzerland; [6]Department of Chemistry, University of Florence, Center for Magnetic Resonance, Sesto Fiorentino (FI), Italy.

Table of contents

1. Sample preparation
2. NMR methods
3. Determination of the contribution factor
4. Calculation of overall sensitivity gain
5. Error estimation
6. Spin diffusion model
7. Tables and figures
8. References

1. Sample preparation

BDPA in glassy matrix: Deuterated chloroform was purchased from Euriso-top and perdeuterated *ortho*-terphenyl (d_{14}-OTP, 98 %) from Cambridge Isotope Laboratories, α,γ-bis-diphenylene-β-phenylallyl (BDPA, 1 : 1 complex with benzene) and 1,1,2,2-tetrachloroethane (TCE, reagent grade, ≥ 98 %) were purchased from Sigma Aldrich and *ortho*-terphenyl (OTP, 98 %) from Alfa Aesar. All chemicals were used as received. Samples containing BDPA in OTP were prepared by mixing 60 mM BDPA with a mixture of 95 % (*w*/*w*) d_{14}-OTP and 5 % (*w*/*w*) OTP on a glass plate. The mixed powders were dissolved in approx. 1 ml of deuterated

chloroform and stirred with a glass rod at room temperature until the solvent was completely evaporated. The resulting red powder was then packed into 1.3 mm zirconia rotors. The mixture was melted inside the closed rotor at about 80 °C, and then rapidly inserted into the cold NMR probe (approx. 100 K) to obtain a homogeneous glassy OTP phase. The same rotor was used for measurements at 9.4 and 18.8 T.

For degassed samples containing BDPA in TCE, TCE was distilled and stored under inert atmosphere. A solution of 60 mM BDPA in TCE was prepared and inserted into a 1.3 mm rotor under inert atmosphere inside a glove box. For non-degassed samples, a solution of 60 mM BDPA was prepared in non-degassed TCE under ambient conditions.

In all rotors, a small amount of ground KBr was added to the bottom of rotor to allow for temperature measurement and control.[1]

Mesoporous Alumina synthesis and impregnation: Mesoporous alumina was prepared according to Ref. 2. The surface area determined by nitrogen physisorption was 550 m^2/g.

About 6 mg of mesoporous alumina were mixed with a dry mixture of about 8 mg of 60 mM BDPA in 95 % (*w*/*w*) d_{14}-OTP and 5 % (*w*/*w*) OTP, prepared as described above by mixing BPDA, d_{14}-OTP and OTP in deuterated chloroform and evaporating the solvent. The powder was then transferred into a 1.3 mm zirconia rotor. The closed rotor was heated in a water bath at about 80 °C for about 5 minutes and then immediately transferred into the cold probe (around 100 K).

2. NMR Methods

The MAS DNP NMR experiments were performed on Bruker Avance III 400 and 800 MHz wide bore spectrometers, equipped with triple resonance 1.3 mm low-temperature MAS probes. DNP was achieved by irradiating the sample with high-power microwaves at a frequency of 263 GHz (9.4 T / 400 MHz) and 527 GHz (18.8 T / 800 MHz), generated by gyrotrons that were operating continuously during the DNP experiments (stability of better than ±1%). The external magnetic field was swept to maximize the OE enhancement and better matching the EPR transition frequency of BDPA with the microwave source ($\omega_e = \omega_{\mu w}$). The sample temperature was adjusted by measuring the ^{79}Br longitudinal relaxation time of a little amount of KBr at the bottom of the rotor.[1]

The OE enhancement at 18.8 T as a function of the microwave power was measured at a MAS frequency of 10 kHz (figure S5) where we observed that ε_H rapidly reaches a plateau at a microwave power above 6 W at the probe base, indicating that the single-quantum EPR

transitions are efficiently saturated at relatively low μw power, as previously reported by Griffin and coworkers.[3]

In order to attenuate the background signal of the probe, one-dimensional ^{1}H experiments were acquired using a DEPTH pulse sequence, consisting of a π/2 pulse followed by two π pulses which are phase cycled according to a combined "EXORCYCLE" and "CYCLOPS" scheme.[4-6] π/2 and π pulses of 2.5 μs and 5.0 μs (100 kHz RF field) were used (see table S1). At 18.8 T, the background signal of the probe could not be fully suppressed using DEPTH experiments. To calculate the enhancement and the contribution factors at this field, the remaining background signal was independently measured using an empty rotor, under otherwise similar conditions and subtracted from the spectra of the OTP solutions (figure S6 and S7). ^{1}H longitudinal relaxation times without microwave ($T_{B,OFF}$) and DNP build-up times with microwave ($T_{B,ON}$) were measured with a standard saturation recovery sequence followed by an echo period before signal acquisition (saturation block— $\tau_{recovery}$— π/2 — τ — π – τ —acquisition).

For ^{1}H–^{27}Al cross polarization (CP) experiments, a low ^{27}Al spin lock RF field less than 20 kHz was employed in order to maximize the efficiency of the CP transfers (see table S2).

Table S1. NMR parameters used for the measurement of the enhancement factors as a function of the spinning frequency and for the measurement of the proton longitudinal relaxation times $T_{B,OFF}$ and DNP polarization build-up times $T_{B,ON}$ on the BDPA/OTP samples.

	400 MHz (9.4 T)	800 MHz (18.8 T)
^{1}H enhancement factors		
Experiment	^{1}H 1D DEPTH	^{1}H 1D DEPTH
Recycle delay	5 s	15 s
π/2 and π pulses	2.5 μs and 5.0 μs	2.5 μs and 5.0 μs
Acquisition time	2 ms	10.2 ms
Complex points acquired	800	2048
Line broadening	200 Hz	200 Hz
^{1}H $T_{B,OFF}$ and $T_{B,ON}$		
Recycle delay	0.2 s	0.1 s
π/2 and π pulses	2.5 μs and 5.0 μs	2.5 μs and 5.0 μs
Acquisition time	2 ms	10.2 ms
Complex points acquired	2048	4096
Line broadening	400 Hz	200 Hz

Table S2. Experimental NMR parameters used for the acquisition of the ^{27}Al NMR using direct excitation and CP MAS experiments recorded on the mesoporous alumina.

^{1}H 1D spin-echo experiments	
$\pi/2$ and π pulses	2.5 μs and 5.0 μs
Acquisition time	10.2 ms
Complex points acquired	2048
Exponential window function	200 Hz
^{1}H – ^{27}Al Cross Polarization	
^{1}H $\pi/2$ pulse	2.5 μs
Contact time	1.7 ms
Linear Ramp	70 % to 100 %
CP matching condition at 40 kHz MAS	42 kHz (^{27}Al), 75 to 107 kHz (^{1}H, 1. SSB condition)
CP matching condition at 10 kHz MAS	42 kHz (^{27}Al), 51 to 73 kHz (^{1}H, 1. SSB condition)
^{1}H RF field during decoupling	100 kHz SPINAL-64 decoupling
Acquisition time	10.2 ms
Complex points	1184
Exponential window function	400 Hz

3. Determination of the contribution factor

The contribution factor θ takes into account all the effects that contribute to reduce the observable signal intensity in the sample due to the presence of a paramagnetic radical. The paramagnetic radical does not affect the signal intensity only because of relaxation, in commonly used nitroxide biradicals also depolarization effects play an important role, especially at high MAS frequency. In solid-state NMR, the spectrum intensity can also be reduced by effects related to the anisotropic terms of the hyperfine Hamiltonian that are not averaged out by the MAS rotation. Without entering in details about the relative roles of these terms, that is still debated inside the DNP community, the contribution factor was measured as described by

Rossini *et al.*[7] according to equation (1) recorded in the absence of μw irradiation using samples of 95% d_{14}-OTP, 5% OTP with 60 mM BDPA or without BDPA and calculated as the ratio of the integrated intensities (*II*) per unit of mass of the aromatic resonance in ^{1}H DEPTH spectra. Recycle delays of five times $T_{B,OFF}$ were used to allow for complete signal relaxation.

$$\theta = \frac{II_{\text{[BDPA in OTP]}}/m_{\text{[BDPA in OTP]}}}{II_{\text{[pure OTP]}}/m_{\text{[pure OTP]}}} \qquad (1)$$

4. Calculation of overall sensitivity gain

Table S3. Enhancement factors, contribution factors and build-up times and overall sensitivity Σ_H at 18.8 T and 40 kHz MAS for BDPA in OTP and AMUPOL in a glycerol-water mixture.

	ε_H	θ	$T_{B,ON}$	Σ_H
60 mM BDPA in 95% d_{14}-OTP and 5% OTP (*w*/*w*)	105	1.0	43.5 s	15.9
10 mM AMUPol in d_8-glycerol/D_2O/H_2O, 60/30/10 (*V*/*V*/*V*) with 0.25 M ^{13}C-proline[8]	56	0.46	9.2 s	8.5

Several calculations have been proposed to assess the overall sensitivity enhancement factor achievable using DNP with respect to conventional NMR experiments on undoped samples at low and room temperature. Different factors need to be considered, including the contribution factor and the ratio between the DNP polarization build-up time constant ($T_{B,ON}$). The nuclear longitudinal relaxation time constant (T_1) of the dry material without radical was assumed to be 1 s. Using equation (2),[7] the parameters of table S3 lead to the overall sensitivity enhancement Σ_H at low temperature of 15.9 and 8.5, for BDPA and AMUPol, respectively. This suggests that the BDPA/OTP solution could provide an efficient alternative at high field and fast MAS to binitroxide polarizing agents being used routinely today.

$$\Sigma_H = (\varepsilon_H)(\theta_H)\sqrt{T_1/T_{B,ON}} \qquad (2)$$

5. Error estimation

The estimation of errors of the enhancements ($\Delta\varepsilon$) were done according to Lelli *et al.*:[9]

$$\Delta\varepsilon = \varepsilon\left(\frac{\Delta I_{on}}{I_{on}} + \frac{\Delta I_{off}}{I_{off}}\right) \qquad (3)$$

where ΔI is the error of the observed signal with an integral of I with and without microwave. The errors are estimated on the basis of the noise level, baseline imperfections and residual background signal which is not completely subtracted. The relative errors are generally higher in the microwave off spectra. The absolute errors are generally higher with higher enhancement factors. We reported the highest absolute error as the error bar for each curve, even if this procedure overestimates the errors of the single points.

To estimate the error of the $T_{B,OFF}$ and $T_{B,ON}$ measurements, the polarization build up curves were fitted with monoexponential curves and the error of the fit was recorded. Fluctuations of the fit were taken into account by removing randomly one point of the measured data and refitting. This was done for all points in the curve. The biggest error was found to be 5 % of $T_{B,OFF}$. This value was applied to all curves, even if this procedure overestimates the errors of some points.

For estimating the error of the contribution factor, a systematic weighing error of the sample has to be added, which becomes significant for 1.3 mm rotors with very small masses. Additionally, phase and baseline subtractions can be ambiguous especially for broad peaks with non-resolved side band patterns at low spinning speeds. We have tested the reproducibility of phase and baseline subtractions between different manipulators and come to the conclusion that small individual differences in phase and baseline subtraction can make up to 10 % of a broad signal. We thus estimate the uncertainty of the contribution factors for these small rotors to be 20 %.

6. Spin diffusion model

The MAS dependence of the DNP enhancement and build-up time is interpreted here using a combination of spin-diffusion and relaxation sinks (source-sink diffusion model). The proposed model invokes the presence of a comparably high concentration of polarizing agent with low or negligible relaxation effect, such as BDPA, and the presence of a very small concentration of relaxing impurities (that could be traces of dissolved O_2, or other paramagnetic impurities) that act as polarization sinks. The high concentration of polarizing agent ensures a rapid and almost uniform distribution of the enhanced polarization in the bulk sample by ^{1}H-^{1}H spin-diffusion but, at the same time, the same spin-diffusion mechanism propagates the polarization towards the relaxation sinks that reduce the polarization to a thermal equilibrium value. The combination of

these two processes affects both the overall enhancement and build-up time of the sample in a way that depends on the magnitude of the spin-diffusion constant, and that in turn scales with the MAS frequency.

This process is analogous to the shortening of the apparent longitudinal relaxation time T_1 (that we call here the build-up time in absence of microwaves: $T_{B,OFF}$) in solid samples doped by the presence of paramagnetic impurities. Bloembergen first showed that the longitudinal build-up time in solids can be reduced by the presence of traces of paramagnetic impurities acting as sinks and by the spin diffusion that propagates the effect to the bulk.[10] This model has been also quantified by Blumberg, Rorschach and others.[11-14] Kessemeier and Norberg investigated this effect in the case of magic angle spinning solid-state NMR.[15] The MAS modulation of the spin-diffusion constant is reflected in the build-up time that is thus a function of the MAS frequency. They reported that, in the regime where the ^{1}H-^{1}H spin-diffusion is slower than the sink relaxation rate, an increase of the MAS frequency can effectively generate an increase of the build-up time because of the progressive isolation of the sinks from the rest of the bulk. Even if their analyses support our hypothesis, the model cannot be directly exported to our case, because of the presence of the DNP hyperpolarization process. We need to interpret both the MAS trends of the enhancement and the build-up time. Thus, we developed a quantitative model correlating the experimental enhancement and the build-up time with the MAS frequency. The model is reported below using two approaches: first an analytical solution, with some reasonable approximations, that fits well the experimental data and also makes it possible to better understand the process quantitatively. Then we report a numerical simulation which is more flexible, and in which more details can be introduced to better fit the experimental data.

6.1 Analytical model

Linear model

The average distance between BDPA molecules in 60 mM BDPA in 95 % deuterated OTP is 3.8 nm. The ^{1}H-^{1}H spin-diffusion from the polarizing agent molecules to the small solvent volume filling the space between radicals is generally fast enough to uniformly distribute the polarization in the bulk in a few ms. So, the enhanced polarization is uniformly distributed in the sample on a time scale much faster than the build-up time. The same cannot be said with respect to the relaxation process induced by sinks, whose concentration is assumed to be thousands of times smaller than the polarizing agent. Consequently, the average volume per sink is thousands of times larger, and much longer time is required to propagate the relaxation effect by spin-

diffusion. The large difference in concentration between polarizing agent and sinks makes it possible to simplify the model: we fix our attention on one sink molecule and assume that the bulk volume (matrix) around the sink contains a uniform distribution of polarizing agent with a uniform build-up time and polarization. The Fick equation (4) can be used to describe the evolution of the polarization building up in the matrix and, at the same time, the polarization flow towards each sink.

$$D \cdot \nabla^2 P(r,t) - \frac{P(r,t)-P_0}{T_{B,RS}} = \frac{\partial P(r,t)}{\partial t} \qquad (4)$$

where $P(r,t)$ is the function describing the polarization distribution during time t and r is the distance from the position of the sink molecule, P_0 is the local equilibrium polarization in absence of sinks (thermal polarization in absence of microwaves or the steady-state limit of the hyperpolarized sample during microwave irradiation). D is the spin-diffusion rate and $T_{B,RS}$ is the build-up time of the polarization in the matrix that includes the radical but without sinks. Here we assume that P_0, D and $T_{B,RS}$ are constant and uniform within the bulk.

In this first model we can consider only one isolated sink that is placed in the position $r = 0$, with the diffusion process occuring in "one dimension" with a linear symmetric model, this makes it possible to simplify the Fick equation:

$$D \cdot \frac{\partial^2 P(r,t)}{\partial r^2} - \frac{P(r,t)-P_0}{T_{B,RS}} = \frac{\partial P(r,t)}{\partial t} \qquad (5)$$

We simplify here the description using a one-dimensional diffusion symmetry because it makes the mathematical description easier, and probably clearer to the reader to understand the physics of the source-sink model. In the following part of this section we present also the analysis considering a spherical symmetry where sinks are particles dispersed into a volume, showing that also in that case the source-sink model agrees with the experimental data. Nevertheless, this linear symmetric model is not just a simplified model, it can be appropriate in the description of systems where the relaxation sinks are not dispersed in a volume but distributed on the surface of the investigated sample. This model can thus be also relevant for the future application of the technique.

From figure S16 we can observe that the enhancement is almost stationary for recycle delays longer than 12-15 s, as used in the present measures of the enhancement. Therefore, we can

analyze the MAS enhancement trend at 18.8 T reasonably assuming that the system has reached the steady state condition $\left(\frac{\partial P(r,t)}{\partial t} = 0\right)$:

$$D \cdot \frac{\partial^2 P(r)}{\partial r^2} - \frac{P(r) - P_0}{T_{B,RS}} = 0 \qquad (6)$$

As boundary condition we assumed that the sink polarization relaxes much faster than the bulk (almost instantaneously) and the fast relaxation keeps the polarization at the sink position fixed at the equilibrium polarization P_{sink}. Then, the solution of (6) for an isolated sink that does not diverge for $r \rightarrow +\infty$ is:

$$P(r, \infty) = (P_{sink} - P_0)\mathrm{e}^{-\frac{r}{\sqrt{DT_{B,RS}}}} + P_0 \qquad (7)$$

where r is the distance from the sink. This function describes an exponential change of polarization as we move away from the sink position. Integrating (7) over a finite volume $0 \leq r \leq L$, where L is half the average sink-to-sink distance (assumed here as the radius of the average matrix volume per sink particle), and using different values of P_0 for the microwaves on and off we can derive the enhancement function as:

$$\varepsilon_\infty = \varepsilon_0 - \frac{\sqrt{DT_{B,RS}}}{L}(\varepsilon_0 - 1)\left(1 - \mathrm{e}^{-\frac{L}{\sqrt{DT_{B,RS}}}}\right) \qquad (8)$$

where ε_∞ is the steady-state enhancement and $\varepsilon_0 = \frac{P_{0,on}}{P_{0,off}}$ is the enhancement in absence of sinks, assuming the enhancement in absence of microwaves to be 1 and without depolarization effects.[1] The radius L reflects the concentration of sink impurities. Notably, the enhancement function depends on the term $\frac{L}{\sqrt{DT_{B,RS}}}$, which is the ratio between the distance L and the "characteristic diffusion length" $\sqrt{DT_{B,RS}}$. The enhancement changes with MAS frequency because increasing the MAS rate reduces the spin diffusion constant D, as a consequence of the attenuation of the dipolar interactions (following the equation (9)),[16] while the intrinsic T_1 remains unperturbed and we assumed that also $T_{B,RS}$ remains constant.

[1] This model can be easily extended to the presence of depolarization, calculating the distribution of polarization in absence of microwaves with eq. (7) and then the corresponding enhancement in the volume L.

$$D(\nu_R) = \frac{D_0}{1+k*\nu_R} \qquad (9)$$

where D_0 is the diffusion constant in the static condition and k is a coefficient scaling the effect of the MAS frequency ν_R.

Figure S1 reports the fit of the experimental enhancement as a function of the MAS frequency of Figure 1a (main text) using eq. (8) and (9). The excellent agreement with the experimental data confirms that the source-sink diffusion model described above can effectively explain the observed experimental data. The sink-to-sink distance ($2L$) is determined in the fitting procedure, and corresponds to a sink concentration of the order of 6.4 μM.

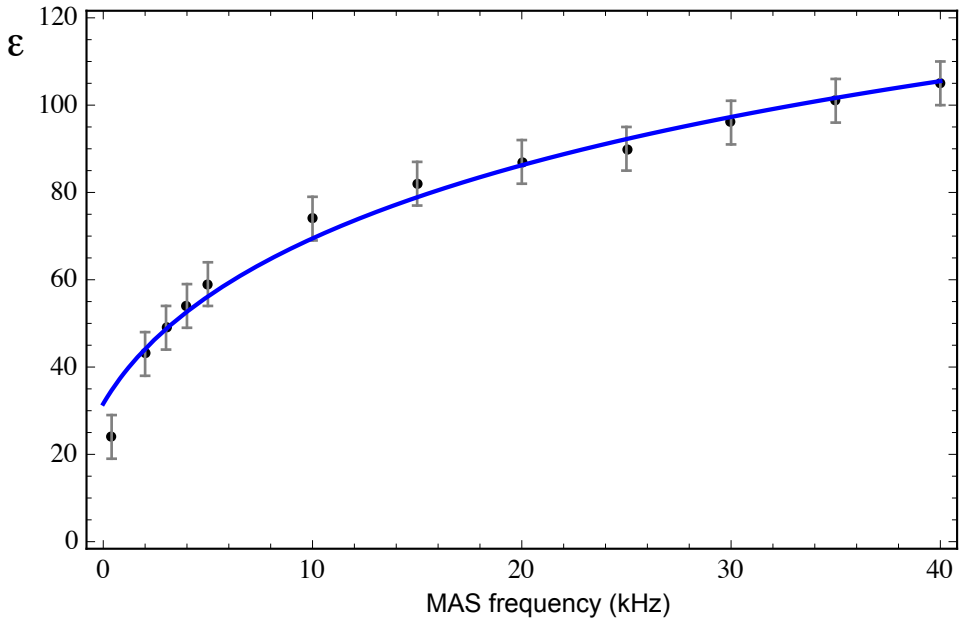

Figure S1. Fitting the experimental enhancement vs MAS frequency with equation (8) and (9). The fitted values are: ε_0 = 203, k = 0.6 ms, D_0 = 2.0 10^{-4} μm^2/s, $T_{B,RS}$ = 68 s and L = 39.5 nm, which corresponds to a sink concentration of 6.4 μM.

To fit the trend of the DNP build-up time we need to solve the time dependent Fick equation (5). Assuming here also that the sink polarization relaxes much faster than $T_{B,RS}$ (for example in the scale of time of a few milliseconds or faster), the solution for equation (5) is:[2]

$$P(r,t) = P_0 - P_0 e^{-\frac{t}{T_{B,RS}}} \mathrm{Erf}\left(\frac{r}{2\sqrt{Dt}}\right) - \frac{(P_0 - P_{sink})}{2}\left[e^{-\frac{r}{\sqrt{DT_{B,RS}}}} \mathrm{Erfc}\left(\frac{r}{2\sqrt{Dt}} - \sqrt{\frac{t}{T_{B,RS}}}\right) + e^{\frac{r}{\sqrt{DT_{B,RS}}}} \mathrm{Erfc}\left(\frac{r}{2\sqrt{Dt}} + \sqrt{\frac{t}{T_{B,RS}}}\right)\right] \qquad (10)$$

[2] Full details about the mathematical derivation of the analytical solutions of the Fick equations here are available upon request to the authors.

where t is the time and Erf and Erfc are the Error function and the complementary Error function, respectively. The polarization as a function of time can be integrated over the volume of length L to obtain the function of the signal build-up as function of time (equation (11)). The observed NMR signal build-up will be proportional to (11): this curve is in fact close to an exponential build-up and it can be fitted with an exponential build-up curve to extract the calculated $T_{\mathrm{B,ON}}$ values.

$$s(t) = P_0 - P_0 \mathrm{e}^{-\frac{t}{T_{B,RS}}} \left\{ \frac{2\sqrt{Dt}\left[\mathrm{e}^{-\frac{L^2}{4Dt}} - 1\right]}{L\sqrt{\pi}} + \mathrm{Erf}\left(\frac{L}{2\sqrt{Dt}}\right) \right\} + \frac{(P_0 - P_{sink})}{2} \frac{\sqrt{DT_{B,RS}}}{L} \left[2\mathrm{Erf}\left(\sqrt{\frac{t}{T_{B,RS}}}\right) - \mathrm{e}^{-\frac{L}{\sqrt{DT_{B,RS}}}} \mathrm{Erfc}\left(\frac{L}{2\sqrt{Dt}} - \sqrt{\frac{t}{T_{B,RS}}}\right) + \mathrm{e}^{\frac{L}{\sqrt{DT_{B,RS}}}} \mathrm{Erfc}\left(\frac{L}{2\sqrt{Dt}} + \sqrt{\frac{t}{T_{B,RS}}}\right) \right] \quad (11)$$

The $T_{\mathrm{B,ON}}$ values can be calculated as a function of the MAS frequency on the basis of (9) and compared to the experimental data of Figure 1a. Figure S2 shows the comparison of the experimental values with those calculated using the same parameters fitted in Figure S1. The proposed model calculates a progressive increase of the build-up time with increasing MAS frequency with a trend that has a reasonably good agreement with the experimental data, and further supports the source-sink diffusion model.

The sink concentration is in the range of μM concentration, confirming that the presence of hardly detectable traces of relaxing impurities, in a sample with long intrinsic relaxation time, is enough to determine the MAS dependence of the enhancement and build-up time.

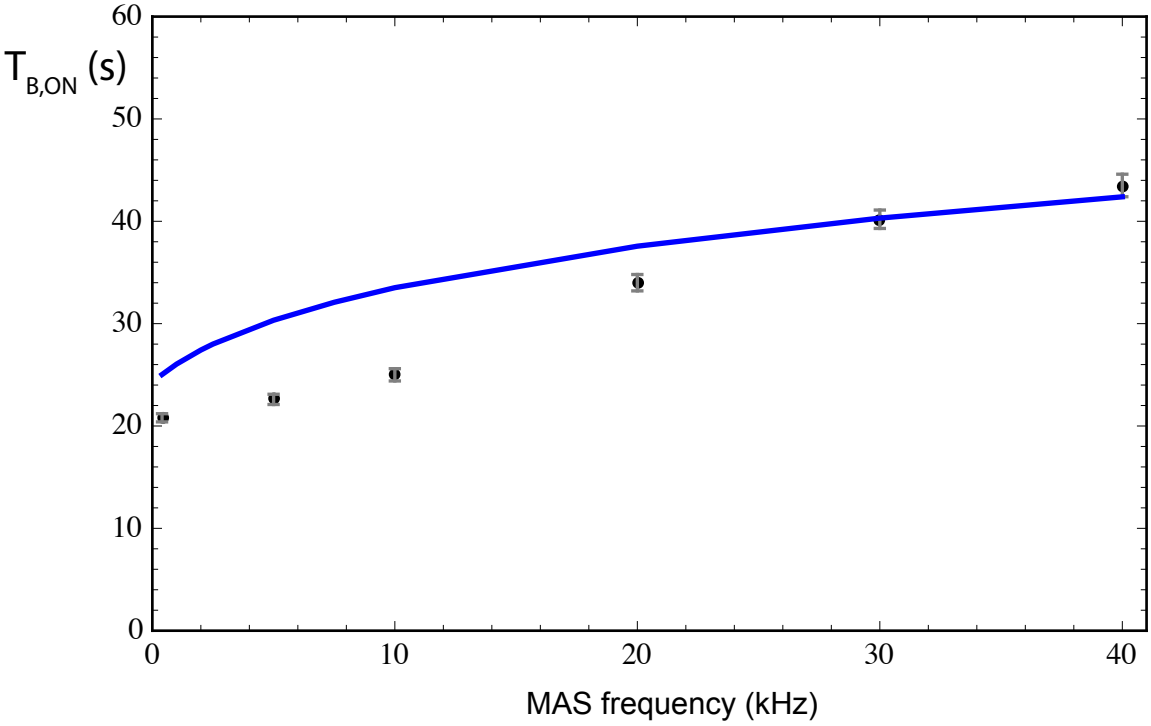

Figure S2. Comparison of the experimental build-up time ($T_{B,ON}$) and the values calculated on the basis of equation (9) and (11). The used parameters were: P_0 = 203, P_{sink} =1, k = 0.6 ms, D_0 = 2.0 10^{-4} μm²/s, $T_{B,RS}$ = 68 s and L = 39.5 nm, which corresponds to a sink concentration of 6.4 μM.

Spherical Model

One of the limitations of the previous model is to consider the spin-diffusion mechanism as a linear diffusion and to consider only one isolated sink. To demonstrate the potential correctness of the source-sink diffusion model we give a description of the model using a spherically symmetric diffusion model. In the following the sink will be modeled as a small relaxation sphere centered at the origin of the coordinate axis. We consider that all the protons within a radius R_0 are rapidly relaxed by the sink to the thermal equilibrium polarization, and that these nuclei do not contribute to spectrum because they are spread over a large spectral window by the strong anisotropic hyperfine interaction. The steady-state Fick diffusion equation in a spherically symmetric system can be described by the following equation:

$$D \cdot \left(\frac{\partial^2 P(r,t)}{\partial r^2} + \frac{2}{r}\frac{\partial P(r,t)}{\partial r}\right) - \frac{P(r,t)-P_0}{T_{B,RS}} = 0 \qquad (12)$$

As boundary conditions we need to impose two constraints: first, in view of the very rapid relaxation of the sink we fix the polarization in the sink surface at radius R_0 to be constant at the value P_{sink}. As a second condition we imposed that the at the radius L, corresponding to ½ of the

average sink-to-sink distances, the flow of polarization is null $\left(\left(\frac{\partial P(r,t)}{\partial r}\right)_L = 0\right)$. This condition implies that at the position L (i.e. in the middle between two sinks) the flow of polarization towards the sink in the origin of the coordinates ($r = 0$) is balanced by the flow of polarization to the neighboring sinks. Thus, this condition is implicitly considering that the system is composed of a dilute distribution of sinks instead of a single isolated sink. The solution of eq. (12) with these boundary conditions is:

$$P(r) = P_0 + k_1 \frac{e^{\frac{-r}{\sqrt{DT_{B,RS}}}}}{r} + k_2 \frac{e^{\frac{r}{\sqrt{DT_{B,RS}}}}}{r}$$

where

$$k_1 = \frac{R_0(P_{sink} - P_0)\left(L - \sqrt{DT_{B,RS}}\right)e^{\frac{L}{\sqrt{DT_{B,RS}}}}}{\left(L - \sqrt{DT_{B,RS}}\right)e^{\frac{L-R_0}{\sqrt{DT_{B,RS}}}} + \left(L + \sqrt{DT_{B,RS}}\right)e^{-\frac{L-R_0}{\sqrt{DT_{B,RS}}}}}$$

$$k_2 = \frac{R_0(P_{sink} - P_0)\left(L + \sqrt{DT_{B,RS}}\right)e^{-\frac{L}{\sqrt{DT_{B,RS}}}}}{\left(L - \sqrt{DT_{B,RS}}\right)e^{\frac{L-R_0}{\sqrt{DT_{B,RS}}}} + \left(L + \sqrt{DT_{B,RS}}\right)e^{-\frac{L-R_0}{\sqrt{DT_{B,RS}}}}} \qquad (13)$$

as in the linear diffusion model detailed above, P_0, D and $T_{B,RS}$ are the equilibrium polarization in absence of sinks, the spin-diffusion rate and the build-up time of the matrix in absence of sinks, respectively. P_0 is considered equal to the thermal equilibrium polarization in absence of microwaves or the steady-state hyperpolarization during microwave irradiation in the sample in absence of sinks. P_0, D and $T_{B,RS}$ are assumed constant and uniform within the bulk. As in the previous model, we observe that the polarization is a function of the ratio between the position r compared to the characteristic diffusion length $\sqrt{DT_{B,RS}}$, and the diffusion constant is sensitive to the MAS frequency (equation (9)). The sample enhancement in the steady state limit (ε_∞) can be evaluated by integrating eq. (13) over the spherical volume $R_0 \leq r \leq L$:

$$\varepsilon_\infty = \varepsilon_0 + \frac{3\sqrt{DT_{B,RS}}}{(L^3 - R_0^3)} \frac{R_0(1 - \varepsilon_0)}{\left(\left(L - \sqrt{DT_{B,RS}}\right)e^{\frac{L-R_0}{\sqrt{DT_{B,RS}}}} + \left(L + \sqrt{DT_{B,RS}}\right)e^{-\frac{L-R_0}{\sqrt{DT_{B,RS}}}}\right)}$$
$$* \left[C_1\left(\left(R_0 + \sqrt{DT_{B,RS}}\right)e^{\frac{-R_0}{\sqrt{DT_{B,RS}}}} - \left(L + \sqrt{DT_{B,RS}}\right)e^{\frac{-L}{\sqrt{DT_{B,RS}}}}\right)\right.$$
$$\left. + C_2\left(\left(L - \sqrt{DT_{B,RS}}\right)e^{\frac{L}{\sqrt{DT_{B,RS}}}} - \left(R_0 - \sqrt{DT_{B,RS}}\right)e^{\frac{R_0}{\sqrt{DT_{B,RS}}}}\right)\right]$$

(14)

where:

$$C_1 = \left(L - \sqrt{DT_{B,RS}}\right)e^{\frac{L}{\sqrt{DT_{B,RS}}}}, \text{ and } C_2 = \left(L + \sqrt{DT_{B,RS}}\right)e^{-\frac{L}{\sqrt{DT_{B,RS}}}} \quad (15)$$

Figure S3 shows the fit of the experimental enhancement data with eq. (14-15) and using eq. (9) for the MAS dependence of the diffusion coefficient.

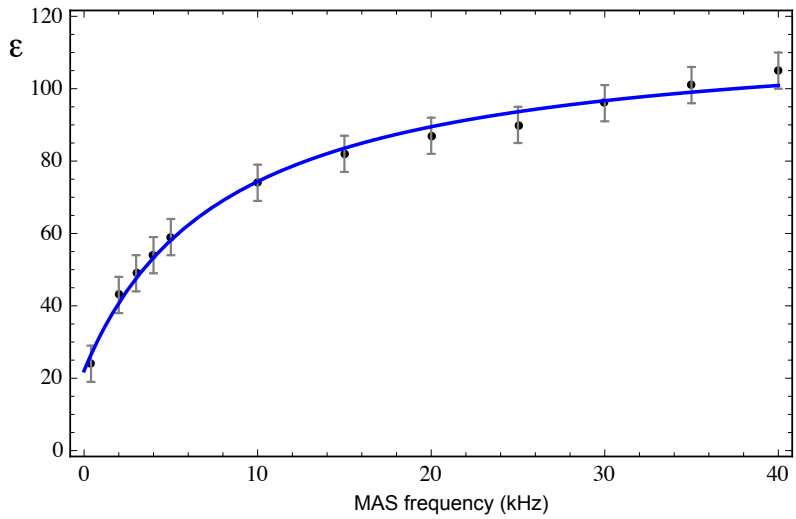

Figure S3. Fitting with of the experimental enhancement data as a function of MAS frequency using eq. (14-15) and eq. (9). The fitted values are: R_0 = 5.0 Å, ε_0 = 117, k = 0.68 ms, D_0 = 2.0 10^{-4} μm²/s, $T_{B,RS}$ = 73 s, and L = 17 nm, which corresponds to a sink concentration of 96 μM.

Notably also this model shows an excellent agreement with the experimental data, with parameters comparable with those of the previous model, demonstrating the quality and the robustness of the source-sink diffusion model.

6.2 Numerical Simulation

Together with the analytical description of diffusion model we also developed a numerical simulation using an approach similar to that described by van der Wel *et al*. and Rossini *et al*.[17-18] The numerical simulation allows to calculate the polarization distribution by solving the Fick equation (5) with the possibility to incorporate additional details such as statistical distributions of sink-to-sink distances or the progressive variation of the spin-diffusion coefficient and relaxation times in the bulk at different distance from the sink. In this model, we consider a linear

diffusion model (eq. (5)) with the sink at the origin (fixed at $r = 0$). The volume around the sink at distance $0 \leq r \leq r_R$ relaxes rapidly with $T_1 = 1.0$ ms (see Figure 2a in the main text and figure S4). This relaxation sink volume is not considered to contribute to the observed signal because their signals are spread over a large spectral window by the strong anisotropic hyperfine interactions.

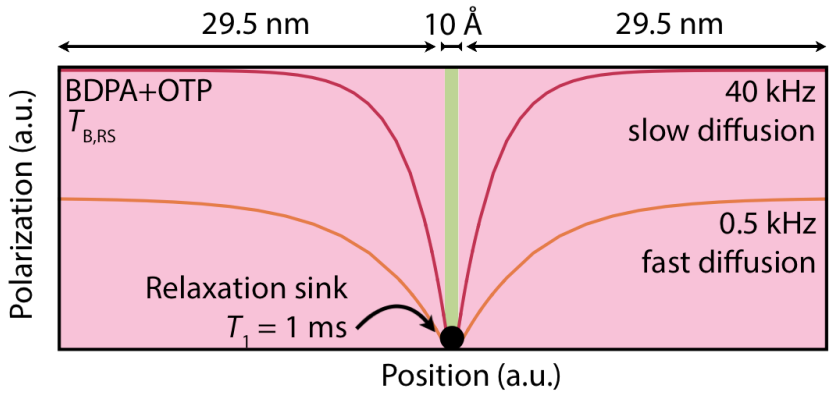

Figure S4. Linear model of the spin diffusion: the bulk matrix with BDPA molecules dissolved in the OTP matrix has a $T_{B,RS} = 73$ s, the paramagnetic impurity acting as relaxation sink has $T_1 = 1.0$ ms. The relaxation sinks are present in a concentration of about 14 μM. A Weibull distribution of sinks was considered, which is centered at 52.4 nm and has a mean value of 60 nm.

The bulk volume contributing to the observed signal, is extended from $r = r_R$ to $r = L$, which is half of the sink-to-sink distance ($2L$), and varies with the MAS frequency following equation (9). A Weibull distribution of sink-to-sink distances was considered according to equation (16)[19] where $P(2L)$ is the probability per length unit, $2L$ is the distance between sinks and a the mean of the distribution (60 nm). The value of L was optimized from the experimental data within the simulation, obtaining a sink-to-sink distance of 60 nm. This value corresponds to a sink concentration of 14 μM. In analogy to the previously described simulation, as a boundary condition we impose that the polarization flow at the sink position was null $\left(\frac{\partial P(r,t)}{\partial r} = 0\right)$, as well the flow is null in the middle of two sinks ($r = L$). The numerical values were adjusted to fit the simulations to the experimental data.

$$P(2L) = \frac{3}{a}\left(\frac{2L}{a}\right)^2 e^{-\left(\frac{2L}{a}\right)^3} \qquad (16)$$

where a and L are in nm. The number "3" has the same units as a and L. The time dependent Fick equation (5), with the above described boundary conditions was solved numerically using equation (9) for the MAS dependence of the diffusion constant. The results of the fitting analysis of the enhancement and build-up time as a function of MAS are reported in the Figure 2b in the main text. The final fitted parameters are $R_0 = 5.0$ Å, $\varepsilon_0 = 260$, $k = 0.6$ ms, $D_0 = 2.0\ 10^{-4}$ m^2/s,

$T_{B,RS}$ = 73 s, and L = 30 nm, which corresponds to a sink concentration of 14 μM. With k = 0.6 ms, we describe a diffusion rate which is divided by about 7 between 4 kHz and 40 kHz. We can clearly see that also in this model we have a very good agreement between the experimental data and the simulation. The agreement between the model and the experimental data seems of lower quality for the points with MAS frequency <5 kHz, this is probably due to the fact that equation (9) is less accurate for slow MAS frequency and a more refined model should be used in this spinning frequency regime.

Notably all these models show that the potential enhancement in absence of sinks, indicated by the parameter ε_0 is significantly higher than the enhancement that is effectively observed. This is relevant is evaluating the real efficacy of a polarizing agent. The build-up time also increases in absence of sinks, but the absolute sensitivity will also be higher in absence of sinks. In a context where the sinks cannot be easily identified and removed, as in our case, spinning at faster MAS is way to increase the overall DNP efficacy.

7. Tables and Figures

Table S4. Summary of the measurements at 18.8 T of 60 mM BDPA in 95 % d_{14}-OTP, 5 % OTP.

MAS / kHz	DNP enhancement of OTP solvent resonance (ε_{1H})	$T_{B,ON}$ / s	$T_{B,OFF}$ / s	Contribution factor θ
0.4	24 ± 5	20.8 ± 0.4	17.1± 0.4	1.01 ± 0.10
2	43 ± 5			
3	49 ± 5			
4	54 ± 5			
5	59 ± 5	22.6 ± 0.5		1.05 ± 0.11
10	74 ± 5	25.0 ± 0.6	19.8 ± 0.5	1.04 ± 0.10
15	82 ± 5			
20	87 ± 5	34.0 ± 0.8	31.7 ± 0.8	1.13 ± 0.10
25	90 ± 5			
30	96 ± 5	40.2 ± 0.9	38.5 ± 0.9	1.09 ± 0.11
35	101 ± 5			
40	105 ± 5	43.5 ± 1.1	40.9 ± 1.0	1.09 ± 0.11

Table S5. Summary of the measurements at 9.4 T of 60 mM BDPA in 95 % d_{14}-OTP, 5 % OTP.

MAS / kHz	DNP enhancement of OTP solvent resonance (ε_{1H})	$T_{B,ON}$ / s	Contribution factor θ
0.4	48 ± 3.5		0.93 ± 0.09
2	57 ± 3.5	35.8 ± 0.9	
5	70 ± 3.5	35.2 ± 0.9	
10	78 ± 3.5	36.2 ± 0.9	1.17 ± 0.12
15	80 ± 3.5	38.8 ± 1.0	
20	80 ± 3.5	40.7 ± 1.0	1.07 ± 0.11
25	88 ± 3.5	42.7 ± 1.1	
30	90 ± 3.5	46.0 ± 1.2	1.13 ± 0.11
35	88 ± 3.5	46.7 ± 1.2	
40	88 ± 3.5	50.4 ± 1.3	1.12 ± 0.11

Table S6: Quadrupolar coupling constants C_Q, isotropic chemical shifts δ_{iso}, width of the chemical shift distribution $\Delta\delta_{iso}$ and relative areas of the three aluminium sites in mesoporous alumina. The data were calculated using the Czjzek model in DMFit.[20-21]

	Al (IV)	Al (V)	Al (VI)
Isotropic chemical shift δ_{iso} / ppm	77.3	39.2	13.3
Width of chemical shift distribution $\Delta\delta_{iso}$ / ppm	8.0	10.3	7.4
Quadrupolar coupling constant C_Q/ MHz	5.77	3.62	5.53
Relative peak area / %	16.8	5.4	77.8

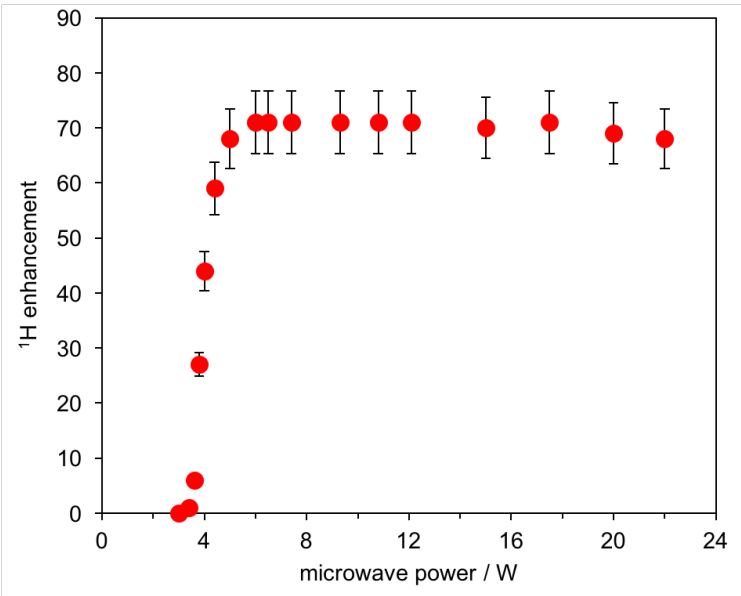

Figure S5. Enhancement factor as a function of microwave power at the base of the probe at 18.8 T and 10 kHz spinning frequency for a sample of 60 mM BDPA in 95% d_{14}-OTP, 5% OTP.

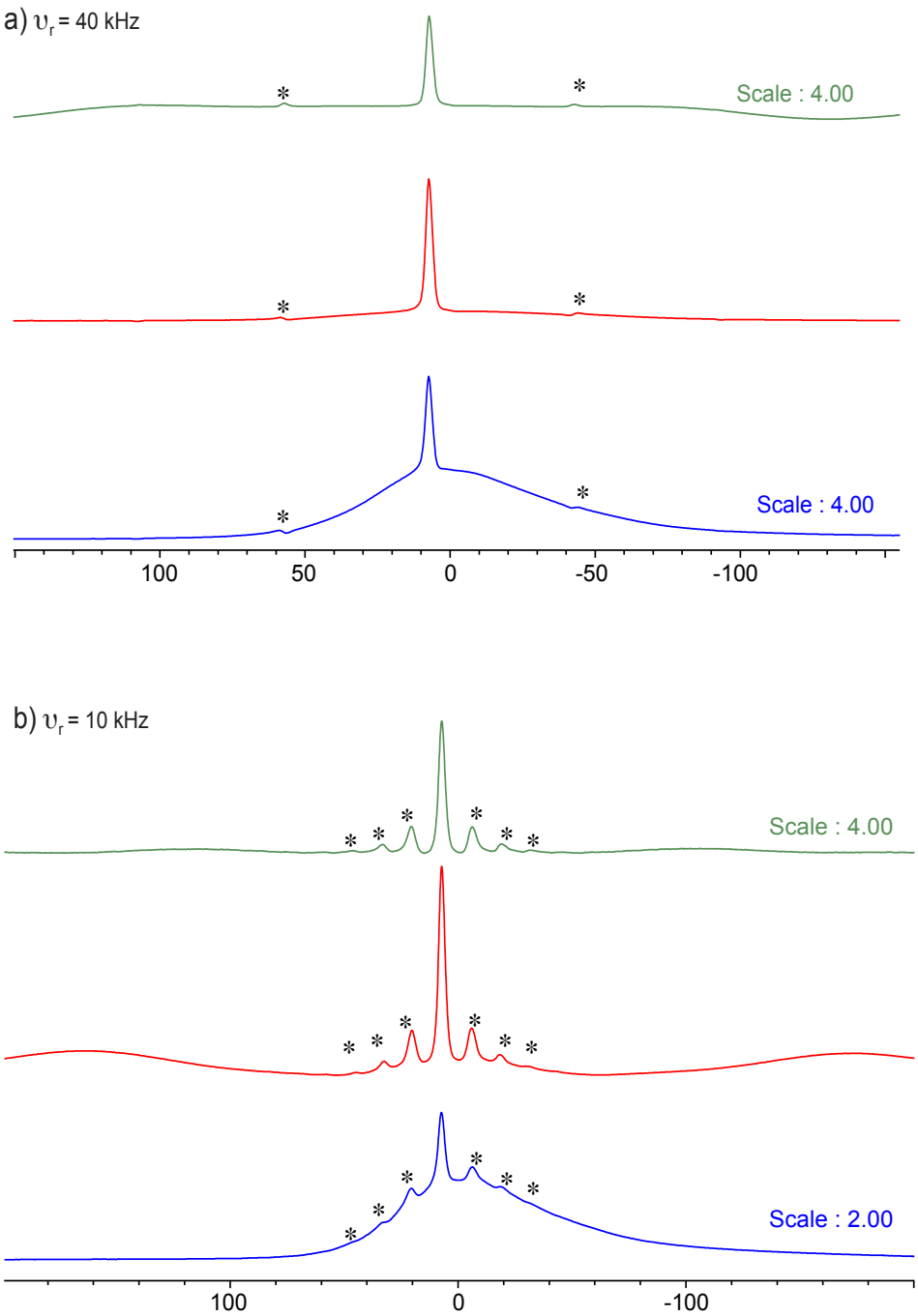

Figure S6. ^{1}H spectra recorded at a) 40 kHz and b) 10 kHz MAS frequencies on 60 mM BDPA in 95% d_{14}-OTP, 5% OTP under microwave irradiation at 18.8 T (sample temperature 128 K ± 3 K). To show the effect of background subtraction, we compare the spectra obtained by single RF pulse (blue), DEPTH pulse sequence (red) and DEPTH pulse sequence with background subtraction (green). The integrals per scans and unit of mass of the background corrected DEPTH spectra were used to calculate the contribution factors. Asterisks denote spinning sideband signals.

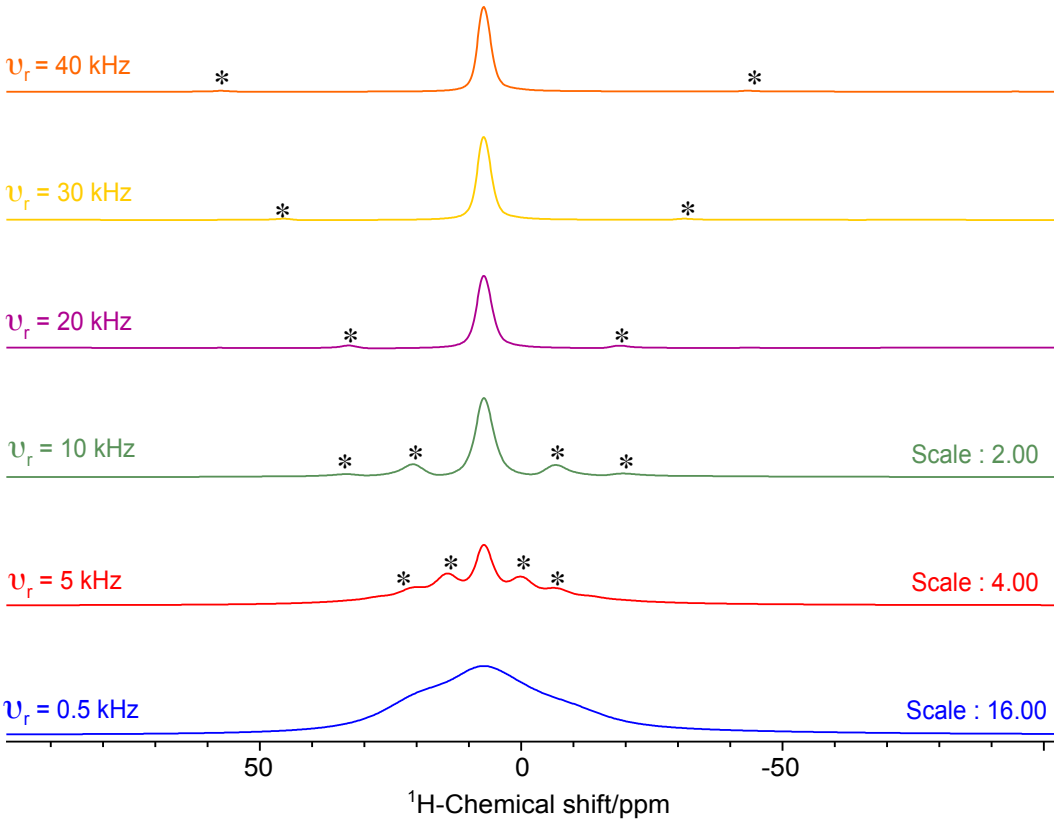

Figure S7. One-dimensional proton DEPTH experiments recorded on a 60 mM BDPA in 95% d_{14}-OTP, 5% OTP at different spinning frequencies under microwave irradiation (18.8 T, sample temperature 128 K ± 3 K) after background subtraction. Asterisks denote spinning sideband signals.

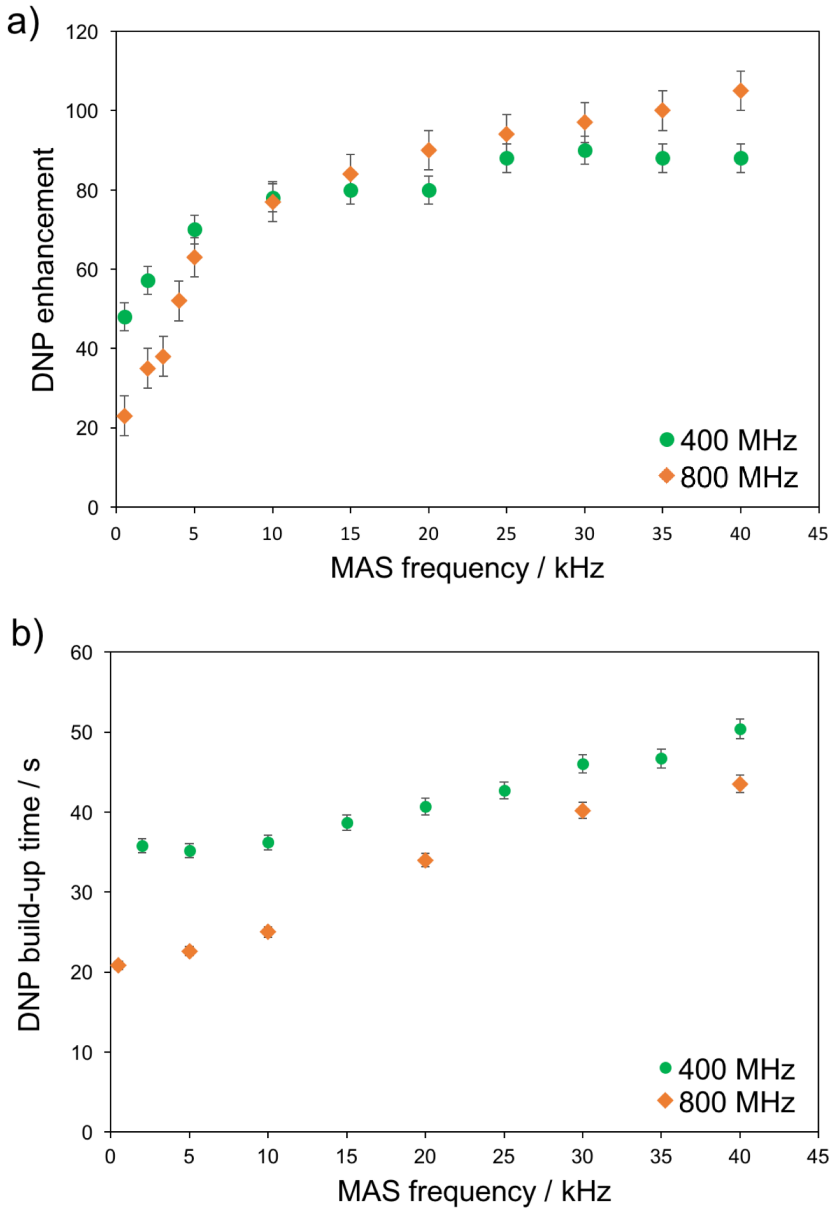

Figure S8. MAS frequency dependence of a) ^{1}H DNP enhancements and b) ^{1}H DNP build-up time $T_{B,ON}$ of 60 mM BDPA in 95% d_{14}-OTP, 5% OTP (*w*/*w*), at 9.45 T (400 MHz / 263 GHz, green circles) and at 18.8 T (800 MHz / 527 GHz, orange diamonds). A constant sample temperature of 128 K ± 3 was maintained over the whole spinning range.

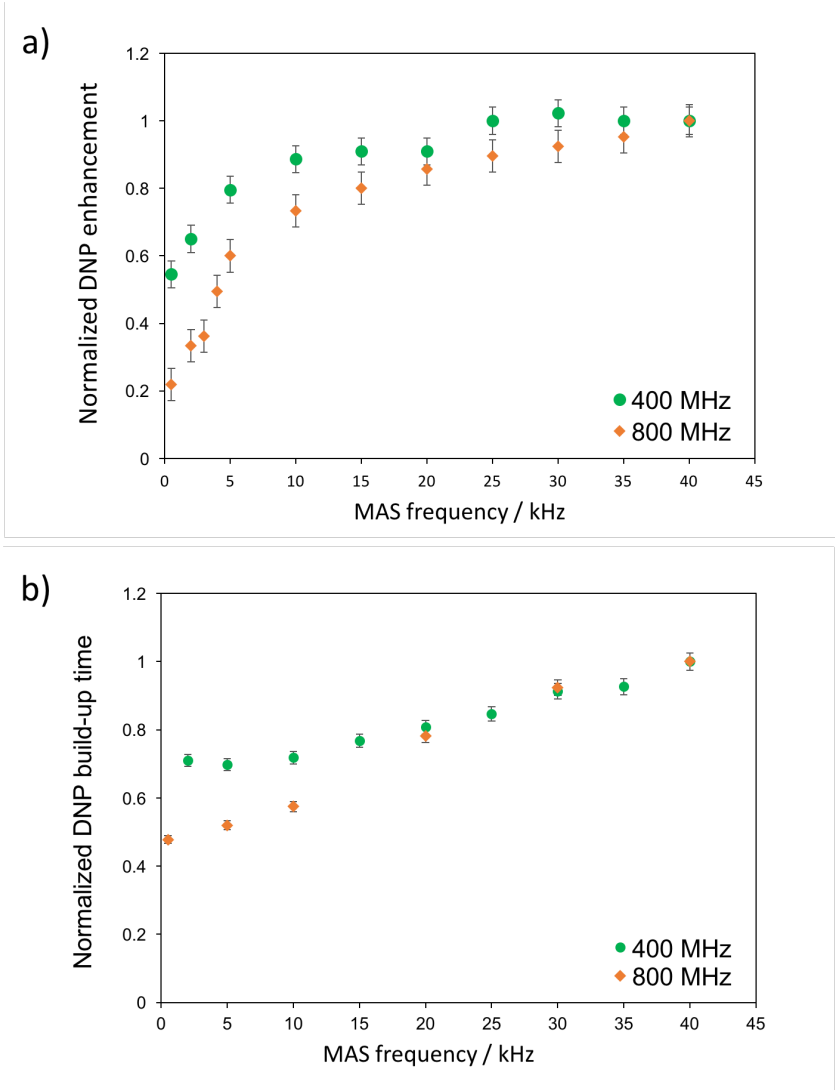

Figure S9. MAS frequency dependence of a) the **normalized** ^{1}H OE DNP enhancements and of b) the **normalized** ^{1}H DNP build-up time $T_{B,ON}$ of 60 mM BDPA in 95% d_{14}-OTP, 5% OTP (*w*/*w*), at 9.4 T (400 MHz / 263 GHz, green circles) and at 18.8 T (800 MHz / 527 GHz, orange diamonds). A constant sample temperature of 128 K ± 3 was maintained over the whole spinning range.

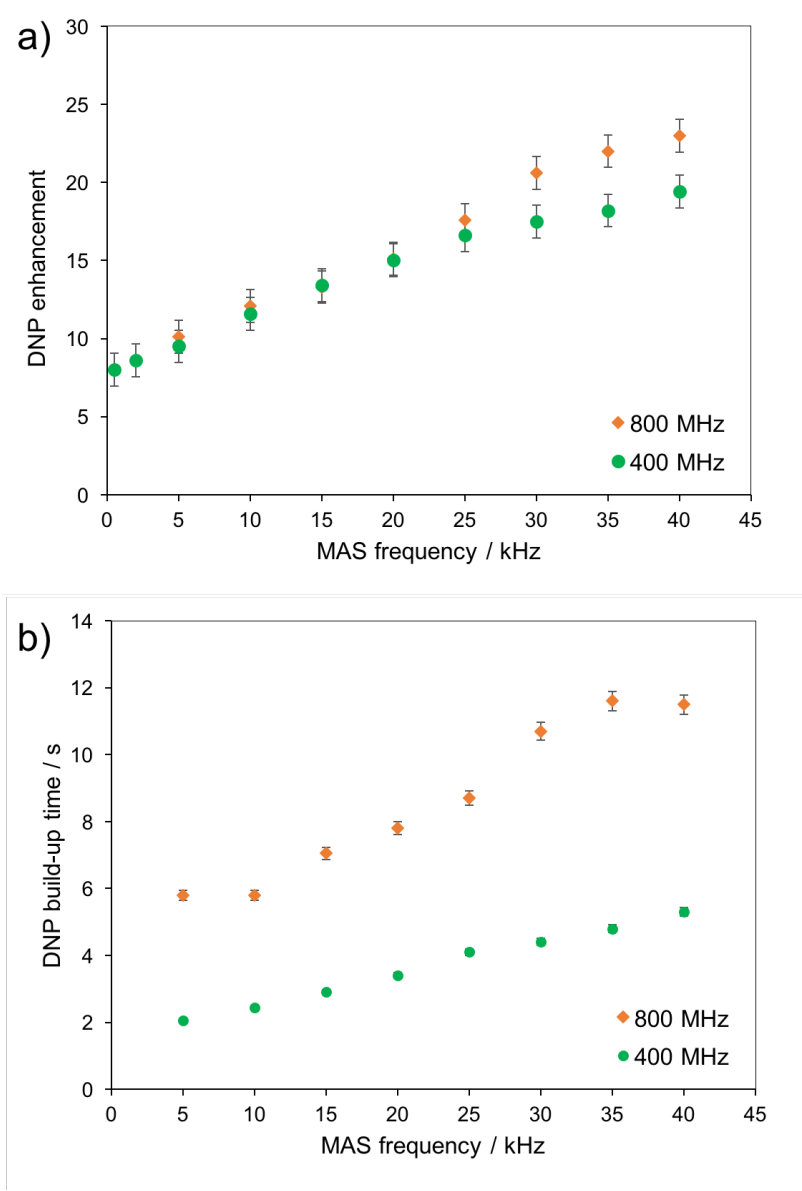

Figure S10. MAS frequency dependence of a) ^{1}H DNP enhancements and b) ^{1}H $T_{B,ON}$ of 60 mM BDPA in 1,1,2,2-tetrachloroethane (TCE). The measurements were done at 9.4 T (400 MHz / 263 GHz, green circles) and 18.8 T (800 MHz / 527. GHz, orange diamonds). A constant sample temperature of 130 ± 3 K was maintained over the whole spinning range.

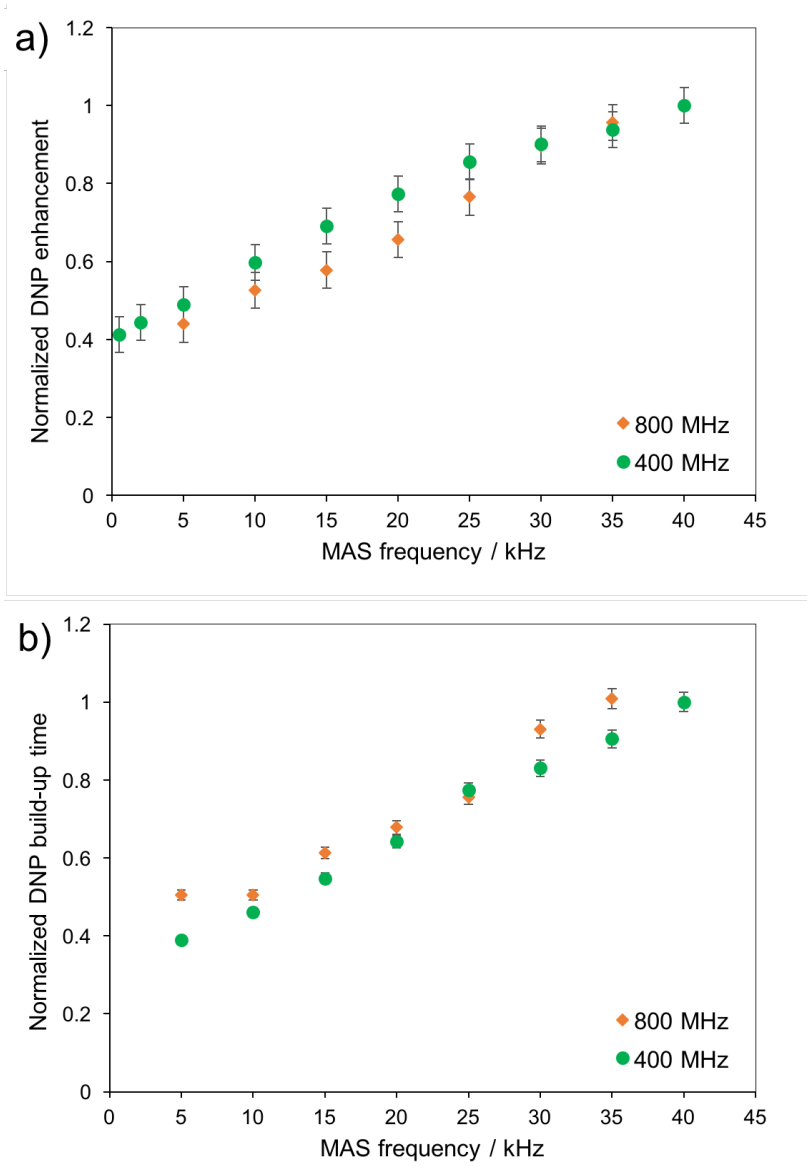

Figure S11. MAS frequency dependence of a) **normalized** ^{1}H DNP enhancements and b) **normalized** ^{1}H $T_{B,ON}$ of 60 mM BDPA in TCE. The measurements were done at 9.4 T (400 MHz / 263 GHz, green circles) and 18.8 T (800 MHz / 527 GHz, orange diamonds). A constant sample temperature of 130 ± 3 K was maintained over the whole spinning range.

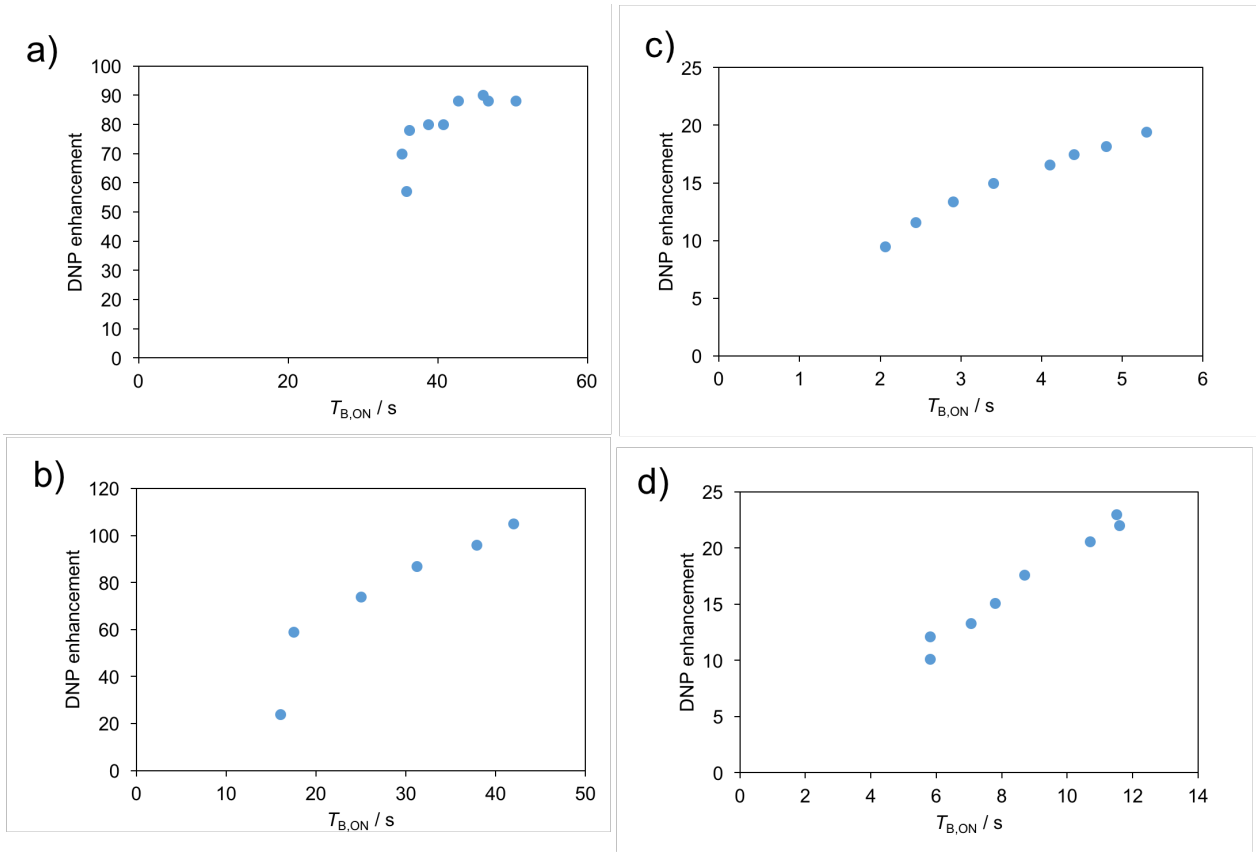

Figure S12. ^{1}H enhancements as function of the respective DNP build up constants $T_{B,ON}$, a) 60 mM BDPA in 95 % d_{14}-OTP, 5 % OTP at 9.4 T (400 MHz), b) 60 mM BDPA in 95 % d_{14}-OTP, 5 % OTP at 18.8 T (800 MHz), c) 60 mM BDPA in TCE at 9.4 T (400 MHz), d) 60 mM BDPA in TCE at 18.8 T (800 MHz). The sample temperature was approx. 128 K and was kept constant over the whole spinning range. The correlation is linear in all cases.

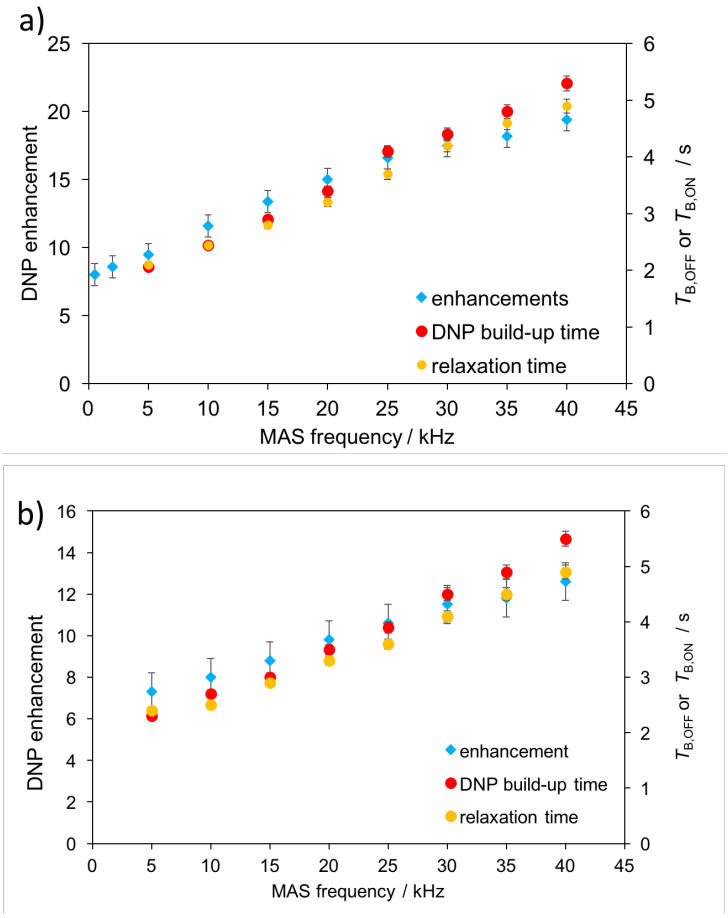

Figure S13. MAS frequency dependence of the ^{1}H OE DNP enhancements (blue diamonds), of the ^{1}H $T_{B,ON}$ (red circles) and of the $T_{B,OFF}$ (yellow circles) of 60 mM BDPA in TCE. The measurements were done at 9.45 T (400 MHz, gyrotron frequency 263 GHz). A constant sample temperature of 130 K ± 3 was maintained over the whole spinning range. a) The sample was prepared with degassed TCE and packed into the rotor under inert atmosphere, b) The sample was prepared with non-degassed TCE and inserted into the cooled probe without degassing. The sample temperature was kept constant at of 130 ± 3 K.

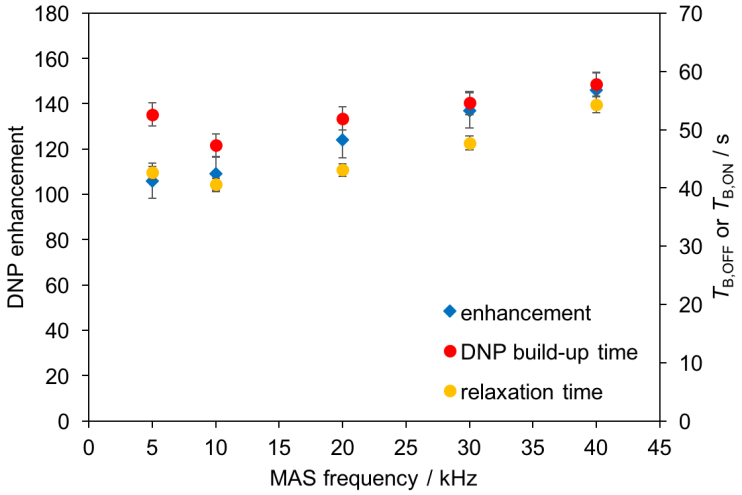

Figure S14. MAS frequency dependence of the ^{1}H Solid Effect (SE) DNP enhancements (blue diamonds), ^{1}H $T_{B,ON}$ (red circles) and $T_{B,OFF}$ (yellow circles) of 60 mM BDPA in 95 % d_{14}-OTP at 9.45 T (400 MHz / 263 GHz). A constant sample temperature of 127 K ± 1 was maintained over the whole spinning range.

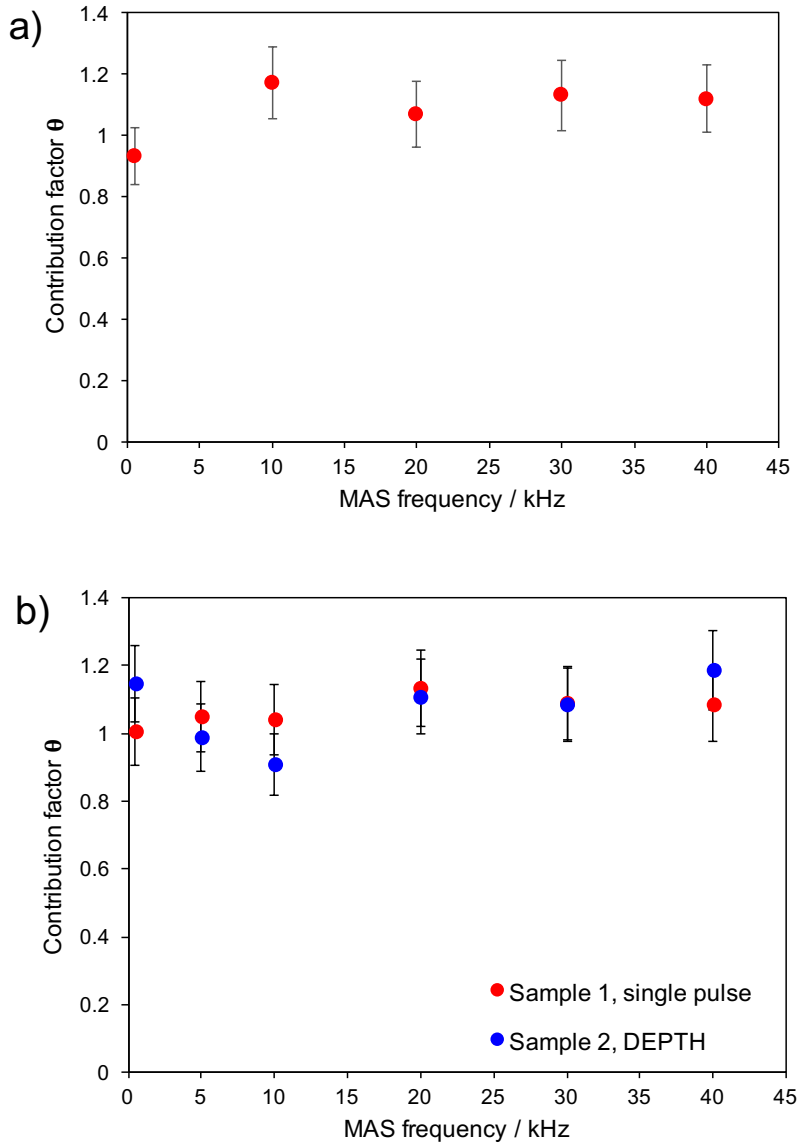

Figure S15. Contribution factor as function of spinning rate of 60 mM BDPA in 95% d_{14}-OTP, 5% OTP (*w*/*w*). a) Measurements at 9.45 T (400 MHz, gyrotron frequency 263 GHz). b) Measurements at 18.8 T (800 MHz, gyrotron frequency 527 GHz). A constant sample temperature of approx. 128 K was maintained over the whole spinning range in all cases. At 800 MHz, two different samples were studied, using either a single pulse (red circles) or a DEPTH pulse sequence (blue circles). All three datasets show the same trend. A background subtraction was applied in all spectra at 18.8 T.

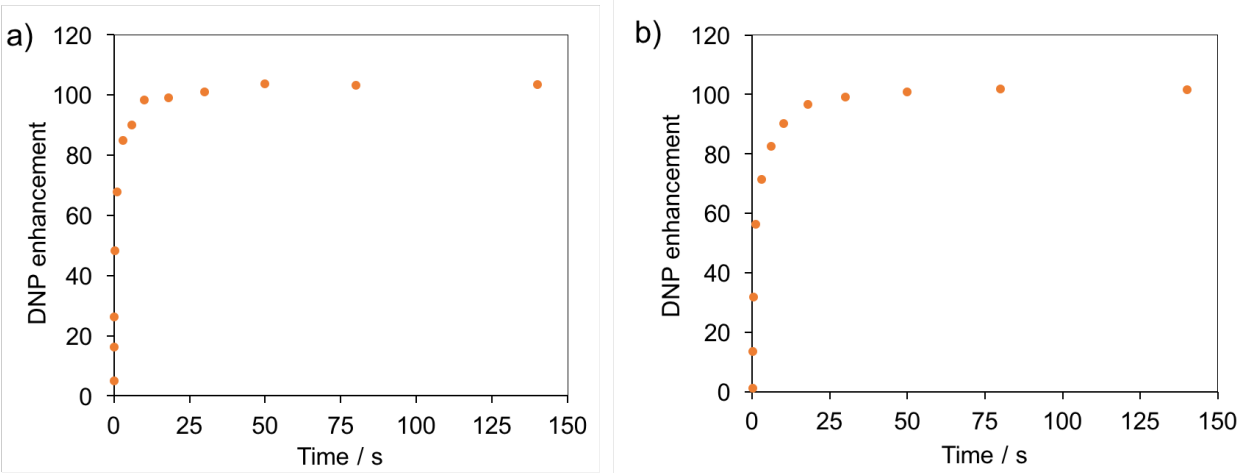

Figure S16. DNP enhancements of 60 mM BDPA in 95 % d_{14}-OTP as function of time at 800 MHz for a) 20 kHz MAS and b) 40 kHz MAS. They were obtained by recording $T_{B,OFF}$ (without microwave) and $T_{B,ON}$ curves (with microwave) as saturation recovery experiments and by dividing the signal intensity of the "microwave on" by the "microwave off" signal for each time increment.

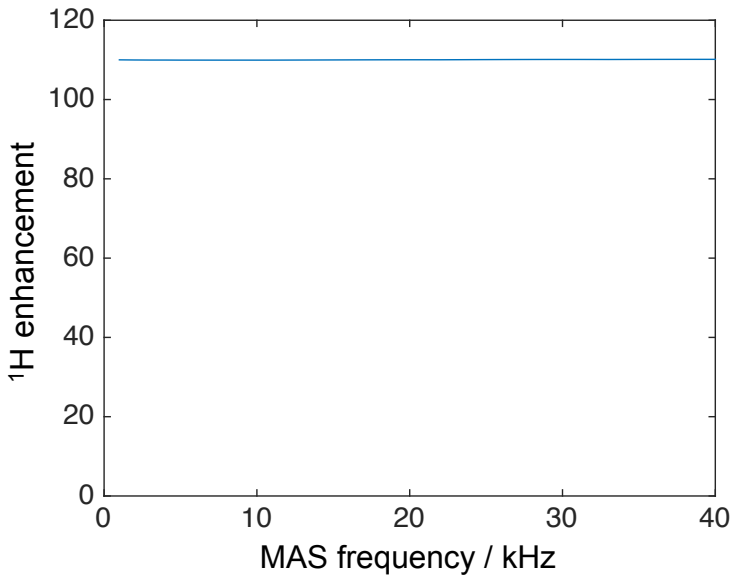

Figure S17: Simulation results for ε_H as function of the MAS frequency at 18.8 T in the case of BDPA radicals acting as both the relaxation source and the sink. No variation of ε_H with MAS is observed.

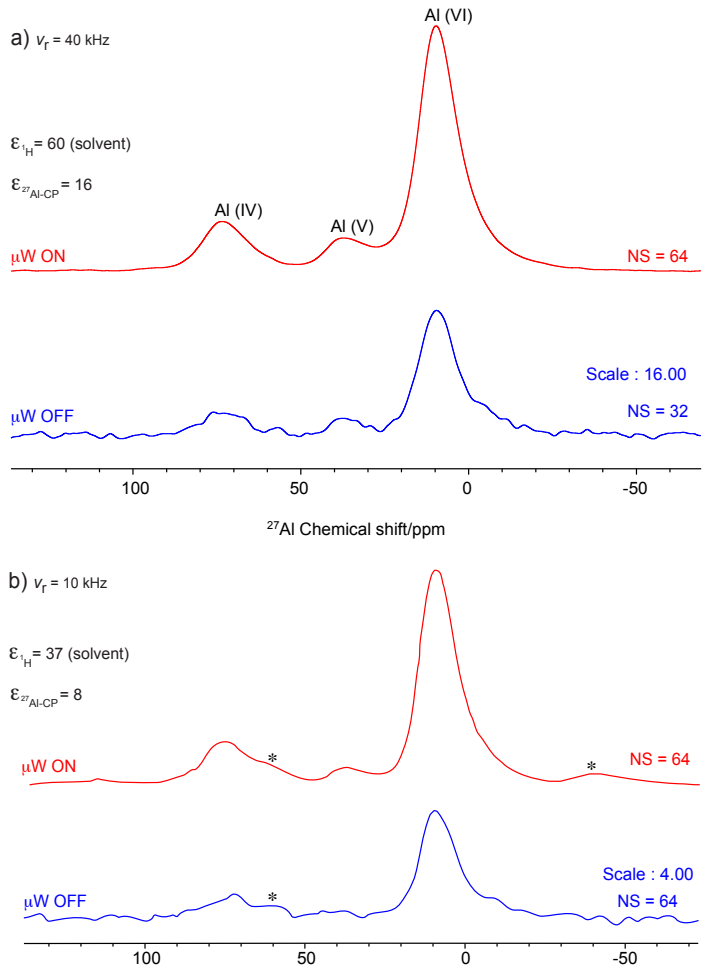

Figure S18. ^{27}Al DNP enhanced CP MAS NMR spectra of mesoporous alumina impregnated with 40 mM BDPA in 95 % d_{14}-OTP at 18.8 T and at a sample temperature of around 128 K with a) 40 kHz and b) 10 kHz spinning frequencies. The spectra were recorded with (red) or without (blue) µw irradiation to induce DNP.

8. References:

1. Thurber, K.; Tycko, R., *J. Magn. Reson.* **2009,** *196*, 84.
2. Vaudry, F.; Khodabaneh, S.; Davis, M. E., *Chem. Mater.* **1996,** *8*, 1451.
3. Can, T. V.; Caporini, M. A.; Mentink-Vigier, F.; Corzilius, B.; Walish, J. J.; Rosay, M.; Maas, W. E.; Baldus, M.; Vega, S.; Swager, T. M.; Griffin, R. G., *J. Chem. Phys.* **2014,** *141*, 064202.
4. Bodenhausen, G.; Freeman, R.; Turner, D. L., *J. Magn. Reson.* **1977,** *27*, 511.
5. Bendall, R. M.; Gordon, R. E., *J. Magn. Reson.* **1983,** *53*, 365.
6. Cory, D. G., Ritchey, W. M., *J. Magn. Reson.* **1988,** *80*, 128.
7. Rossini, A. J.; Zagdoun, A.; Lelli, M.; Gajan, D.; Rascón, F.; Rosay, M.; Maas, W. E.; Copéret, C.; Lesage, A.; Emsley, L., *Chem. Sci.* **2012,** *3*, 108.
8. Chaudhari, S. R.; Berruyer, P.; Gajan, D.; Reiter, C.; Engelke, F.; Silverio, D.; Copéret, C.; Lelli, M.; Lesage, A.; Emsley, L., *Phys. Chem. Chem. Phys.* **2016,** *18*, 10616.
9. Lelli, M.; Chaudhari, S. R.; Gajan, D.; Casano, G.; Rossini, A. J.; Ouari, O.; Tordo, P.; Lesage, A.; Emsley, L., *J. Am. Chem. Soc.* **2015,** *137*, 14558.
10. Bloembergen, N., *Physica* **1949,** *15*, 386.
11. Khutsishvili, G. R., *Proc. Inst. Phys. Adac. Sci. Georgia* **1956,** *4*, 3.
12. De Gennes, P. G., *J. Phys. Chem. Solids* **1958,** *7*, 345.

13. Blumberg, W. E., *Phys. Rev.* **1960,** *129*, 79.
14. Rorschach Jr., H. E., *Physica* **1964,** *30*, 38-48.
15. Kessemeier, H.; Norberg, R. E., *Phys. Rev.* **1967,** *155*, 321.
16. Maricq, M. M.; Waugh, J. S., *J. Chem. Phys.* **1979,** *70*, 3300.
17. Rossini, A. J.; Zagdoun, A.; Hegner, F.; Schwarzwälder, M.; Gajan, D.; Copéret, C.; Lesage, A.; Emsley, L., *J. Am. Chem. Soc.* **2012,** *134*, 16899.
18. van der Wel, P. C.; Hu, K. N.; Lewandowski, J.; Griffin, R. G., *J. Am. Chem. Soc.* **2006,** *128*, 10840.
19. Weibull, W. A., *J. Appl. Mech.* **1951,** *18*, 293.
20. Massiot, D.; Fayon, F.; Capron, M.; King, I.; Le Calvé, S.; Alonso, B.; Durand, J.-O.; Bujoli, B.; Gan, Z.; Hoatson, G., *Magn. Reson. Chem.* **2002,** *40*, 70.
21. d'Espinose de Lacaillerie, J.-B.; Fretigny, C.; Massiot, D., *J. Magn. Reson.* **2008,** *192*, 244.